Spectral ellipsometry investigation of $Zn_{0.53}Cd_{0.47}Se$ lattice matched to InP

Todd Holden,* Prakhya Ram, and Fred H. Pollak*,†
Physics Department and New York State Center for Advanced Technology in Ultrafast Photonic Materials and Applications, Brooklyn College of the City University of New York, Brooklyn, New York 11210

J. L. Freeouf
Interface Studies, Inc., Katonah, New York 10536

B. X. Yang and M. C. Tamargo*
Chemistry Department and New York State Center for Advanced Technology in Ultrafast Photonic Materials and Applications, City College of the City University of New York, New York, New York 10031
(Received 6 November 1996; revised manuscript received 27 January 1997)

Spectral ellipsometry at 300 K, in the range 0.8–5.5 eV, has been used to study the bulk and surface oxide properties of a molecular-beam-epitaxy grown $Zn_{0.53}Cd_{0.47}Se$/InP film ($\approx 1\ \mu$m thick). We have observed the direct gap E_0, which exhibits a well-defined excitonic structure, its spin-orbit split component $E_0+\Delta_0$, as well as the spin-orbit split E_1, $E_1+\Delta_1$ doublet. The experimental data over the entire measured spectral range (after oxide removal) have been fit using a model dielectric function based on the electronic energy-band structure near critical points plus excitonic and Coulomb enhancement effects. The influence of a native oxide on the optical properties also was investigated. [S0163-1829(97)02428-4]

I. INTRODUCTION

ZnSe-based semiconductor alloys are important materials from both fundamental and applied perspectives, due to their potential in the fabrication of blue-green laser devices.[1] Currently, the only reported cw blue-green laser involved ZnSe-based alloys grown nearly lattice matched to GaAs substrates, which contained a strained layer $Zn_xCd_{1-x}Se$ active region. Laser diodes with lifetimes over 100 h have been demonstrated recently.[2] This development has largely relied on the reduction of defect density such as stacking faults and dislocations,[3,4] which occur at the interface of GaAs and ZnSe. The degradation most likely still remains as defects at the II-VI/III-V interface that propagate into the active region, aided by the presence of strain in the $Zn_xCd_{1-x}Se$ quantum well. Entirely lattice matched structures can be fabricated on InP substrates, thus possibly improving the reliability of the devices.

A detailed understanding of the bulk and surface optical properties of these materials is essential in order to make the best selection. However, in spite of its significance, very little work has been done on the optical properties of $Zn_{0.53}Cd_{0.47}Se$ lattice matched to InP.[5,6] Several authors have reported ellipsometric studies on closely related materials such as ZnSe (bulk),[7,8] ZnSe/GaAs(001),[9–11] $Zn_xCd_{1-x}Se$/GaAs(001),[12–14] and zinc blende CdSe.[12,15] Only a preliminary ellipsometric study of $Zn_{0.53}Cd_{0.47}Se$/InP(001) in the range 1.5–5.5 eV has been presented.[6] Fits to various models have been presented in Refs. 8–10 and 12–15. However, none of these investigations accounted for the data around the fundamental direct gap (E_0) with the correct exciton plus band-to-band Coulomb enhanced (BBCE) line shape but rather used an exciton plus a one-electron band-to-band parabolic form. Also, in Refs. 8, 9, and 15 the E_1, $E_1+\Delta_1$ doublet was not resolved. The measurements of Refs. 9, 10, and 15 were performed without removal of the native oxide.

For this paper, spectral ellipsometry in the range 0.8–5.5 eV has been used to study the bulk complex dielectric function $\epsilon(E)$ $[=\epsilon_1(E)+i\epsilon_2(E)]$ of a molecular-beam-epitaxy (MBE) grown $Zn_{0.53}Cd_{0.47}Se$/InP film ($\approx 1\ \mu$m thick). We have investigated films both as received and after a HF etch to remove the native oxide. The experimentally measured dielectric function (after oxide removal) has been fit over the entire range of measurement using a model based on the electronic energy-band structure near critical points. Excitonic and Coulomb enhancement effects were included not only at the fundamental gap E_0, but also its spin-orbit split component $E_0+\Delta_0$ as well as the spin-orbit split E_1, $E_1+\Delta_1$ doublet. In addition, the effects of the native oxide on the optical properties has been evaluated.

II. EXPERIMENTAL DETAILS

The sample was fabricated in two Riber 2300P MBE chambers, one for II-VI growth and the other for III-V growth, connected by UHV modules. The films were grown on a not intentionally doped ($n\approx 5\times 10^{17}$ cm^{-3}) InP buffer layer (500 Å) on a n^+-type InP(001) substrate. Details about the growth are described in Yang *et al.*[16]

The complex dielectric function $\epsilon(E)$ was measured in the range from 0.8 to 5.5 eV at room temperature using an Instruments, SA spectroscopic phase modulated ellipsometer.[17–19] Light from a 125-W xenon arc lamp was passed through an optical fiber to a Glan-type polarizer made of two calcite precision prisms then to a rectangular-shaped fused silica photoelastic modulator. The light is then reflected from the sample and becomes elliptically polarized, after which the light passes through a second fixed polarizer (oriented at 45° from the first polarizer and modulator) then a second optical fiber, and then a monochromater. For the data above 1.5 eV, a double monochromater was used, with a photomultiplier detector mounted on the monochromater

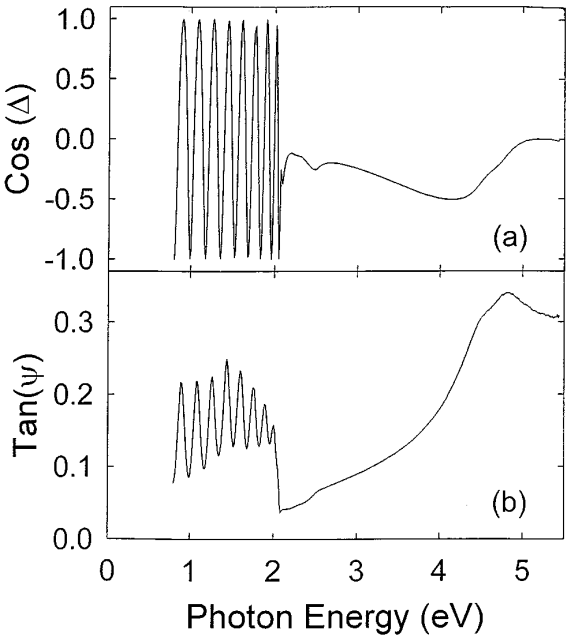

FIG. 1. The ellipsometric data (a) cos(Δ) and (b) tan(ψ) of $Zn_{0.53}Cd_{0.47}Se$/InP (oxide removed) measured at an angle of incidence of 70° in the range 0.8–5.5 eV.

exit slit, while for the data from 0.8 to 1.5 eV, a different monochromater was employed and the exiting light passed through an optical fiber to an $In_xGa_{1-x}As$ detector.

The alloy sample was measured as received, then etched in a 10% solution of HF in H_2O, as suggested by Liu *et al.*,[20] until the spectra showed no change after further etching (about 1 min). A Br/methanol etch was also used on a few samples, but this resulted in a rough surface morphology. After etching, the sample was then placed in a dry methanol bath for transfer into a glove bag filled with dry N_2. While under dry nitrogen, the sample was removed from the methanol bath, blown dry by nitrogen, placed upon the sample stage, aligned, and measured at three angles of incidence (65°, 70°, and 75°). An experimental difficulty arose in maintaining the sample under dry nitrogen during the measurement: exposure of the modulation head of our ellipsometer to this nitrogen resulted in a large ($\approx$20%) change in measured dielectric functions. Care was therefore taken to prevent such exposure by means of small entrance holes for the incident beam, spacing between the entrance aperture to the glove bag and the modulation head, and a small fan to divert nitrogen leaving the bag. Such care is not required with the more common rotating analyzer/polarizer ellipsometer systems, and the reasons for this effect on the modulation system remain unclear.

Figure 1 shows the room-temperature ellipsometric data for (a) cos(Δ) and (b) tan(ψ) measured at an angle of incidence of 70° in the range 0.8–5.5 eV. The large oscillations below the fundamental band gap E_0 (about 2 eV) are interference fringes. Interference effects above the band gap become negligible as the penetration depth is much less than the film thickness.

The data analysis requires several steps, the first step of which is to determine the layer thickness. This value can be determined from large interference fringes below the fundamental band gap, which are periodic in the product of the

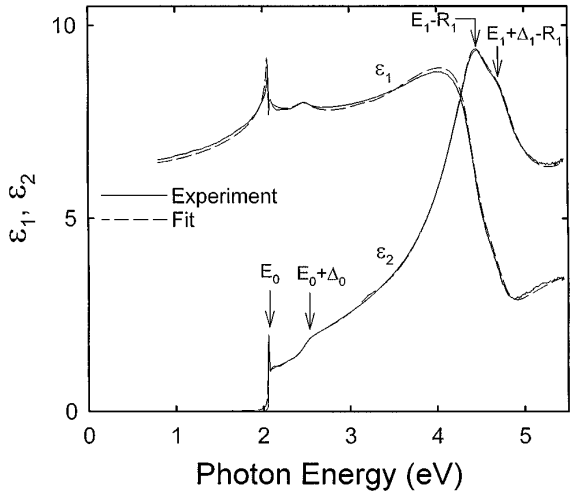

FIG. 2. The solid lines are the experimental values of ϵ_1 and ϵ_2 (oxide removed) in the range 0.8–5.5 eV. The dashed lines are the fits to Eqs. (2)–(5).

refractive index times the layer thickness divided by the wavelength. While we do not know either the index or the thickness *a priori*, we begin by assuming that the index is a constant; since the thickness is also constant, this means that at least six periods of the interference fringes must be explained for the measured wavelength variation by only two parameters: a fixed index of refraction and the inferred layer thickness. This treatment was then refined by using a Sellmeier model[21] for the behavior of the index of refraction (or ϵ_1) in the transparent region below the band gap:

$$\epsilon_1(E) = n_0^2 + [bE_a^2/(E_a^2 - E^2)]. \tag{1}$$

This appraisal adds two more free parameters that must be obtained. A least-squares analysis leads to the following best fit parameters: n_0^2 (=5.4), b (=0.81), and E_a (=2.5 eV), which yielded a thickness of 1.34 ± 0.02 μm. Using a Philtec Instruments sectioner the dimension of the epilayer was found to be 1.30 ± 0.1 μm.

Next, using a multilayer ellipsometric analysis program, the system $Zn_xCd_{1-x}Se$/InP was modeled using this thickness to find the real and imaginary components of dielectric constant that best explained the experimental data for all three angles; this analysis was performed sequentially for each wavelength within the program. This process was repeated for different assumed thickness, and a range of thickness was found that minimized the residual error. The final obtained thickness was 1.31 μm, in good agreement with the physical determination of the layer dimension. For the energy range at the onset of absorption, where the absorption coefficient cannot be presumed zero but the optical response still must account for the substrate, further ambiguity arose in that more than one combination of real and imaginary dielectric functions were equally consistent with the data. We chose the pair most consistent with the less ambiguous results from higher and lower energies. Although more complicated interface structures could have been analyzed, the samples discussed here were grown on InP buffer layers and no need for an extra interface layer was found.

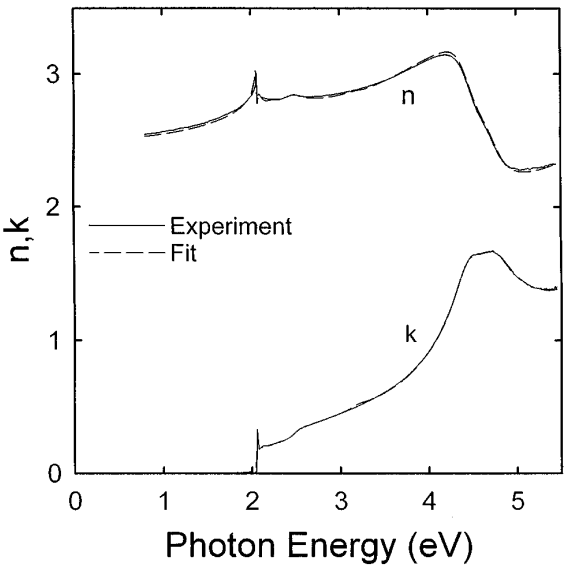

FIG. 3. The solid lines are the experimental values of n and k (oxide removed) in the range 0.8–5.5 eV. The dashed lines are the fits.

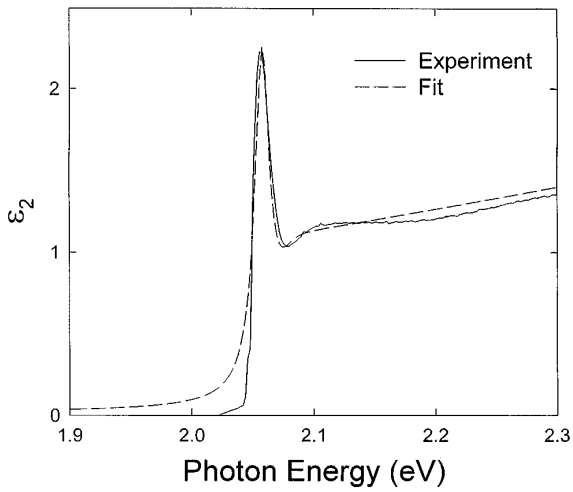

FIG. 4. The solid line is the experimental value of ϵ_2 (oxide removed) in the region of E_0. The dashed line is the fit to Eq. (2).

III. RESULTS AND ANALYSIS

For purposes of discussion we consider the band structures of ZnSe (Ref. 22) and zinc blende CdSe,[12] respectively, since the band structure of $Zn_xCd_{1-x}Se/InP$ has not been calculated. The fundamental absorption edge of these materials corresponds to three-dimensional (3D) M_0 direct transitions from the highest valence band to the lowest conduction band at the Γ point (i.e., $\Gamma_{15}^v-\Gamma_1^c$, in single group notation). The spin-orbit interaction splits the Γ_{15}^v valence band into Γ_8^v and Γ_7^v (splitting energy Δ_0). The corresponding transitions at $\mathbf{k}=0$ are labeled E_0 $[\Gamma_8^v(\Gamma_{15}^v)-\Gamma_6^c(\Gamma_1^c)]$ and $E_0+\Delta_0$ $[\Gamma_7^v(\Gamma_{15}^c)-\Gamma_6^v(\Gamma_1^c)]$, respectively. The spin-orbit interaction also splits the $L_3^v(\Lambda_3^v)$ valence band into $L_{4,5}^v(\Lambda_{4,5}^v)$ and $L_6^v(\Lambda_6^v)$. The corresponding 2D M_0 transitions are labeled E_1 $[L_{4,5}^v(L_3^v)-L_6^c(L_1^c)$ or $\Lambda_{4,5}^v(\Lambda_3^v)-\Lambda_6^c(\Lambda_1^c)]$ and $E_1+\Delta_1$ $[L_6^v(L_3^v)-L_6^c(L_1^c)$ or $\Lambda_6^v(\Lambda_3^v)-\Lambda_6^c(\Lambda_1^c)]$, respectively. The E_2 feature is due to transitions along [110] (Σ) or near the X point, at an energy between 6–7 eV.

A. General features

Shown by the solid lines in Figs. 2 and 3 are values of ϵ_1, ϵ_2 and n (real), k (imaginary) components of the complex index of refraction, respectively, as a function of photon energy E obtained from an analysis of the data of Fig. 1. Displayed by the solid line in Fig. 4 is ϵ_2 in the vicinity of E_0. The direct gap exhibits a very well-defined excitonic structure even at 300 K. In Figs. 2 and 3 the spin-orbit split component $E_0+\Delta_0$ also is seen. There is a very well-resolved $E_1, E_1+\Delta_1$ doublet in the region around 4.5 eV.

The line shape in the vicinity of $E_0, E_0+\Delta_0$ and $E_1, E_1+\Delta_1$ has been fit by a Lorentzian broadened (a) excitonic and (b) relevant BBCE profiles, i.e., 3D M_0 for the former two features and 2D M_0 for the latter two. In order to account for the experimental curves over the entire photon energy range it was also necessary to include the influence of (a) the $\Gamma_8^v-L_6^c$ indirect transition and (b) the E_2 transitions.

B. Model dielectric function

The dielectric properties of a crystal are known to be strongly connected with its energy-band structure. Transitions involving these energy bands, including relevant excitonic effects, are responsible for all the structure in the optical constants at readily available photon energies. In the model that we have employed, the dielectric function $\epsilon(E)$ is approximated as a sum of several components, each of which is an explicit function of energy and represents a contribution from the neighborhood of a critical point (CP) in the joint density of states. For the $E_0, E_0+\Delta_0$ and $E_1, E_1+\Delta_1$ features we have explicitly taken exciton effects into account. As required $\epsilon_1(E)$ and $\epsilon_2(E)$ are Kramers-Kronig (KK) transforms of each other.

1. E_0 and $E_0+\Delta_0$ features

The data near the E_0 band gap have been fit to a function which contains Lorentzian broadened (a) excitonic and (b) 3D M_0 BBCE contributions:[23–25]

$$\epsilon_2(E)=\mathrm{Im}\left(\frac{A}{E^2}\left\{\sum_n \frac{2R_0}{n^3}\left[\frac{1}{E_{n,0}^{\mathrm{ex}}-E-i\Gamma_{n,0}^{\mathrm{ex}}}+\frac{1}{E_{n,0}^{\mathrm{ex}}+E+i\Gamma_{n,0}^{\mathrm{ex}}}\right]+\int_{-\infty}^{\infty}\left[\frac{\theta(E'-E_0)}{1-e^{-2\pi z_1(E')}}-\frac{\theta(-E'-E_0)}{1-e^{-2\pi z_2(E')}}\right]\frac{dE'}{E'-E-i\Gamma_0}\right\}\right), \tag{2a}$$

where A is a constant, E_0 is the energy of the direct gap, R_0 is the effective Rydberg energy $[=(E_0-E_{1,0}^{\mathrm{ex}})]$, $E_{n,0}^{\mathrm{ex}}$ and $\Gamma_{n,0}^{\mathrm{ex}}$ are the energy and broadening of the nth state of the exciton, Γ_0 is the broadening parameter for the band-to-band transition, $z_1(E)=[R_0/(E\text{-}E_0)]^{1/2}$, $z_2(E)=[R_0/(-E-E_0)]^{1/2}$, and $\theta(x)$ is the unit step function. The energy of the nth exciton state $E_{n,0}^{\mathrm{ex}}$ is given by Refs. 23–25, while for the broadening parameter we have used the empirical formula[24]

$$E_{n,0}^{\mathrm{ex}} = E_0 - \frac{R_0}{n^2}, \quad n = 1,2,3,\ldots, \tag{2b}$$

$$\Gamma_{n,0}^{\mathrm{ex}} = \Gamma_0 - \frac{\Gamma_0 - \Gamma_{1,0}^{\mathrm{ex}}}{n^2}. \tag{2c}$$

Once the final form of ϵ_2 was determined, ϵ_1 was evaluated from the KK relations. The precise expression we have employed is presented as Eq. (A7) in the Appendix and produced line shapes very similar to those previously used.[24,25]

The dashed line in Fig. 4 is a least-squares fit to Eqs. (2) with values of the relevant parameters listed in Table I.

The $E_0+\Delta_0$ feature has also been described by broadened excitonic and BBCE components, with parameters similar to those used for the E_0 feature, i.e., Eqs. (2) with $A \rightarrow B$, $E_0 \rightarrow E_0+\Delta_0$, $R_0 \rightarrow R_{\mathrm{so}}$, $\Gamma_{n,0}^{\mathrm{ex}} \rightarrow \Gamma_{n,\mathrm{so}}^{\mathrm{ex}}$, and $\Gamma_0 \rightarrow \Gamma_{\mathrm{so}}$.

2. E_1 and $E_1+\Delta_1$ features

The $E_1, E_1+\Delta_1$ CPs are of the 2D M_0 type with an exciton whose contribution to $\epsilon_2(E)$ can be derived in a manner similar to that for E_0. For the E_1 feature we can write[26,27]

$$\epsilon_2(E) = \mathrm{Im}\left(\frac{C_1}{E^2} \left\{ \sum_n \frac{4R_1}{(2n-1)^3} \left[\frac{1}{E_{n,1}^{\mathrm{ex}} - E - i\Gamma_{n,1}^{\mathrm{ex}}} + \frac{1}{E_{n,1}^{\mathrm{ex}} + E + i\Gamma_{n,1}^{\mathrm{ex}}} \right] \right.\right.$$
$$\left.\left. + \int_{-\infty}^{\infty} \left[\frac{\theta(E'-E_1)}{1+e^{-2\pi z_3(E')}} \frac{-\theta(-E'-E_1)}{1+e^{-2\pi z_4(E')}} \right] \frac{dE'}{E'-E-i\Gamma_1} \right\} \right), \tag{3a}$$

where C_1 is a constant, E_1 is the energy of the gap, R_1 is the effective 2D Rydberg energy $[=(E_1 - E_{n,1}^{\mathrm{ex}})]$, $E_{n,1}^{\mathrm{ex}}$ and $\Gamma_{n,1}^{\mathrm{ex}}$ are the energy and broadening of the nth state of the exciton Γ_1 is the broadening parameter for the band-to-band transition, $z_3(E) = [R_1/4(E-E_1)]^{1/2}$, and $z_4(E) = [R_1/4(-E-E_1)]^{1/2}$. The energy of the nth exciton state $E_{n,1}^{\mathrm{ex}}$ is given by[26,27]

$$E_{n,1}^{\mathrm{ex}} = E_1 - \frac{R_1}{(2n-1)^2}, \quad n = 1,2,3,\ldots . \tag{3b}$$

The quantity ϵ_1 was then determined from the KK transformation of Eq. 3(a) in a procedure similar to that used for the E_0 transition [Eq. (A12)].

The $E_1+\Delta_1$ feature also has been described by excitonic and BBCE components, with parameters similar to those used for the E_1 feature, with $C_1 \rightarrow C_2$ and $E_1 \rightarrow E_1+\Delta_1$, etc.

In practice, only a single broadening parameter Γ_1 was used for the excitonic as well as the BBCE components for both the E_1 and $E_1+\Delta_1$ transitions and also the same effective 2D Rydberg (R_1) was used for both features.

In order to initialize the parameters for the E_1 and $E_1+\Delta_1$ features, the first ($d\epsilon/dE$) and second ($d^2\epsilon/dE^2$) derivatives of the experimental dielectric function with respect to the energy were calculated numerically. These results are shown by the solid lines in Figs. 5 and 6, respectively.

The first and second derivatives of our expressions for the dielectric functions for the E_1 and $E_1+\Delta_1$ resonances were obtained analytically [Eqs. (A16) and (A17), respectively] and fit to the relevant numerical derivative of the data, as displayed by the dashed lines in Figs. 5 and 6, respectively. The fit to $d^2\epsilon/dE^2$ allowed us to determine the broadening parameter (Γ_1) and the exciton energies (E_1-R_1 and $E_1+\Delta_1-R_1$) as well as the products C_1R_1 and C_2R_1. However, due to the large exciton binding energy, the BBCE contribution to $d^2\epsilon/dE^2$ was very small making it difficult to determine R_1 from this data. The quantity $d\epsilon/dE$ is more sensitive to the Rydberg enabling us to obtain an initial value of $R_1 \approx 250$ meV. This is in reasonable agreement with a theoretical value of 300 meV for ZnSe.[28]

The first derivative spectrum (Fig. 5) shows a significant background that can be seen on the low-energy side of E_1 and also a small background on the high-energy side. As will be discussed in more detail below, these differences have been ascribed to the influence of the $\Gamma_{8,v}$-L_6^c indirect band gap (E_{ind}) and the E_2 transitions, respectively.

3. Indirect Γ_8^v-L_6^c band gap (E_{ind})

The contribution of the Γ_8^v-L_6^c indirect transition (see Figs. 1 and 2) can be modeled by[29]

$$\epsilon(E) = D_{\mathrm{ind}} \left\{ -2 \left[\frac{E_{\mathrm{ind}}}{E+i\Gamma_{\mathrm{ind}}} \right]^2 \ln\left(\frac{E_c}{E_{\mathrm{ind}}} \right) + \left[1 + \frac{E_{\mathrm{ind}}}{E+i\Gamma_{\mathrm{ind}}} \right]^2 \ln\left(\frac{E+i\Gamma_{\mathrm{ind}}+E_c}{E+i\Gamma_{\mathrm{ind}}+E_{\mathrm{ind}}} \right) + \left[1 - \frac{E_{\mathrm{ind}}}{E+i\Gamma_{\mathrm{ind}}} \right]^2 \ln\left(\frac{E+i\Gamma_{\mathrm{ind}}-E_c}{E+i\Gamma_{\mathrm{ind}}-E_{\mathrm{ind}}} \right) \right\}, \tag{4}$$

where $D_{\rm ind}$ is the amplitude, $E_{\rm ind}$ and $\Gamma_{\rm ind}$ are the indirect band gap and broadening parameter, respectively, while E_c is a cutoff energy ($=E_1-R_1$). We have taken $E_{\rm ind}=3.9$ eV based on the band structures of ZnSe and zinc blende CdSe.

4. E_2 feature

The E_2 peak is difficult to analyze as it does not correspond to a single, well defined CP.[8,29] Thus, the E_2 structure (not observed) has been characterized as a damped harmonic oscillator:[8,29]

$$\epsilon(E)=\frac{F_2}{[(1-\chi_2^2)-i\chi_2\gamma]}, \tag{5}$$

with $\chi_2=E/E_2$, where F_2 is the strength parameter and γ is a dimensionless broadening parameter. The E_2 feature was not observed, but was expected to lie between the E_2 structure of ZnSe near 6.6 eV and that of zinc blende CdSe near 6.0 eV. The energy of E_2 was taken to be 6.35 eV for the fit.

5. Total dielectric function

The model presented above can be used to fit the experimental dispersion of $\epsilon(E)$ over the entire range of the measurements. The total dielectric function was found by summing the expressions given in the previous four sections, i.e., Eqs. (2)–(5) and their relevant KK transforms. A constant, $\epsilon_{1\infty}$, was added to the real part of the dielectric constant to account for the vacuum plus contributions from higher-lying energy gaps (E_0', E_1', etc.).[8,29] The parameters such as A, B, R_0, etc. were used as adjustable constants for the calculation of both $\epsilon_1(E)$ and $\epsilon_2(E)$. Shown by the dashed lines in Fig. 2 is a least-squares fit to Eqs. (2)–(5) with the obtained parameters given in Table I. Note that there is excellent agreement between the experiment and fit. The values of the interband transitions E_0, $E_0+\Delta_0$ as well as excitonic E_1-R_1, $E_1+\Delta_1-R_1$ features are denoted by arrows. For comparison purposes we have also listed in Table I the numbers for ZnSe from Ref. 8.

Displayed in Figs. 7 and 8 are the individual contributions to $\epsilon_1(E)$ and $\epsilon_2(E)$, respectively, of the various transitions. They were obtained from Eq. (2) (and its KK transform) for the 3D exciton and BBCE 3D M_0 E_0,$E_0+\Delta_0$ transitions, Eq. (3) (and its KK transform) for the 2D exciton and BBCE 2D M_0 E_1,$E_1+\Delta_1$ transitions, Eq. (4) for the indirect $\Gamma_8^v-L_6^c$ contribution, and Eq. (5) for the E_2 resonances.

After the initial fitting it was noted that ϵ_2 still had a significant value below the E_0 gap, so that a linear cutoff was introduced for the $E_{\rm ind}$, E_1, E_1+D_1, and E_2 contributions to ϵ_2 to eliminate this effect by using the equation

$$\epsilon_{2,\rm co}=\epsilon_2\frac{E-E_0}{E_{\rm co}-E_0}, \tag{6}$$

where we have used $E_{\rm co}=3.2$ eV. The quantity ϵ_1 was obtained by a numerical KK analysis of Eq. (6).

C. Oxide effects

The effect of oxide formation on the optical constants also has been observed. Oxide thickness and surface roughness has a large effect on the pseudodielectric function. The measured pseudodielectric function $\langle\epsilon\rangle$ of an as-received sample (with oxide) is compared to an etched sample (without oxide) in Fig. 9. The effect of the oxide is (a) to lower $\langle\epsilon_2\rangle$ in the region around E_1,$E_1+\Delta_1$ and increase it at lower energies and (b) to diminish $\langle\epsilon_1\rangle$ for all photon energies in our spectral range.[17]

To gain further information about the native oxide we have taken the values of ϵ (without the oxide) and added the effects of this layer by means of a three-phase model.[16] The only relevant oxide optical constants available are for ZnO, which were employed. Shown by the solid lines in Fig. 10 are the experimental values of $\langle\epsilon\rangle$ for the as received sample. The dashed lines are a least-squares fit simulation yielding a 20 Å thickness of ZnO. Lee *et al.*[14] have reported a similar oxide thickness in their study of $Zn_xCd_{1-x}Se$/GaAs. Despite the small thickness obtained for the oxide layer, it should be noted that it appears to be a very robust and stable covering, as evidenced by its relative lack of reactivity to various etchants.

IV. DISCUSSION

For ϵ_1 in Fig. 2 we have used the KK inversion of Eqs. (2) and (3) and the real components of Eqs. (4) and (5) plus $\epsilon_{1\infty}=1.53$. Note that there is an excellent agreement over the entire spectral range of the measurement. These fits yielded the values of the relevant parameters listed in Table I. These values are somewhat different in relation to Ref. 6 (1.5–5.4 eV) because of the extended range of the measurements in this paper (0.8–5.5 eV). For comparison purposes we also present in Table I numbers for ZnSe from Ref. 8.

In contrast to other ellipsometric studies of related materials such as ZnSe (bulk),[7,8] ZnSe/GaAs(001),[9–11] $Zn_xCd_{1-x}Se$/GaAs(001),[12–14] and zinc blende CdSe (Refs. 12 and 15) we have used a Lorentzian broadened (a) excitonic and (b) relevant BBCE profiles for not only E_0,$E_0+\Delta_0$ but also for E_1,$E_1+\Delta_1$. This approach has enabled us to extract the relevant Rydbergs for the exciton associated with these various transitions. Although Kim and Sivananthan[10] took into account excitons for these four features in ZnSe they used only a one-electron expression for the band-to-band transitions. To improve their fit the authors of Ref. 10 added a Gaussian term to the broadening. Adachi and Taguchi[8] used only an excitonic profile for E_1,$E_1+\Delta_1$. References 8 and 10 did not extract the Rydberg R_1. In Ref. 12 the effects of the exciton at both E_0,$E_0+\Delta_0$ and E_1,$E_1+\Delta_1$ were accounted for on the basis of a Slater-Koster ''contact'' potential, which results in a phase shift between the real and imaginary components of the complex dielectric function and their derivatives. The discrete nature of the excitons was not considered. In Refs. 9, 13, and 14 the data were fit with a simple harmonic-oscillator model.

The nature of the E_1,$E_1+\Delta_1$ transitions in diamond- and zinc blende-type semiconductors has been the subject of considerable investigation. It is well known that these features contain not only a band-to-band component but also a strong excitonic contribution, even at room temperature.[26,30] Efforts to fit the optical and derivative optical properties with an exciton plus a one-electron band-to-band profile, without taking into account the proper BBCE form, has necessitated

TABLE I. Material parameters used in the calculation of the optical constants of $Zn_{0.53}Cd_{0.47}Se/InP$. Values for ZnSe from Ref. 8 also are listed.

Parameter	$Zn_{0.53}Co_{0.47}Se$	ZnSe
E_0 (eV)	2.078 ± 0.003	2.69
A $(eV^{1.5})$[a]	11 ± 0.5	49/23.4[b]
R_0 (meV)	20 ± 2	17
Γ_0 (meV)	10 ± 2	30
$\Gamma_{0,ex}$ (meV)	7.5 ± 1	30
$E_0+\Delta_0$ (eV)	2.52 ± 0.02	3.10
B $(eV^{1.5})$[b]	7.3 ± 0.7	24.5/11.7[d]
R_{so} (meV)	20 ± 6	17
$\Gamma_{so}/\Gamma_{so,ex}$ (meV)	70 ± 6	30[c]
E_1-R_1 (eV)	4.42 ± 0.01	4.75
C_1 (eV^2)	14.8 ± 1	48.3[d]
R_1 (meV)	270 ± 50	
Γ_1 (meV)	245 ± 5	370
$E_1+\Delta_1-R_1$ (eV)	4.72 ± 0.02	5.05
C_2 (eV^2)	9.0 ± 1	27.4[d]
E_{nd} (eV)	3.9[e]	
F_{ind}	730 ± 70	
Γ_{ind} (meV)	650 ± 70	
E_c (eV)	4.42[f]	
E_2 (eV)	6.35[e]	6.7
D_2	1.55 ± 0.15	1.6
γ	0.24 ± 0.07	0.2
$\epsilon_{1\infty}$	1.53 ± 0.15	1.2

[a]Reference 8 used different amplitude constants for the exciton and band-to-band features.
[b]Parabolic band-to-band transition, not BBCE.
[c]Γ_{so} only.
[d]Exciton only; evaluated using our value of R_1.
[e]Fixed.
[f]Set equal to E_1-R_1.

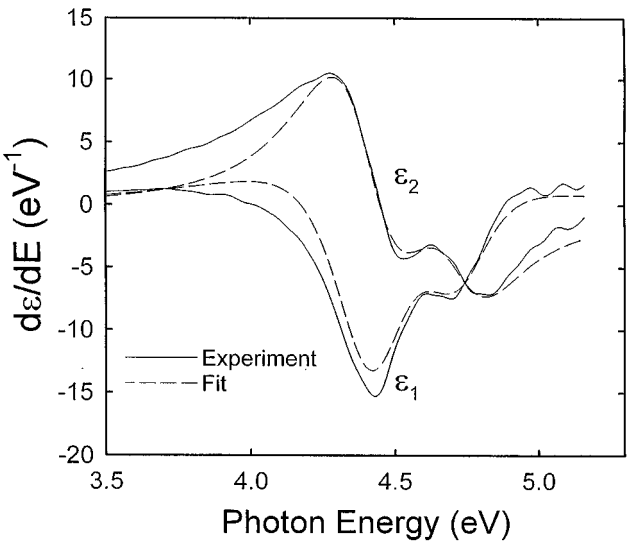

FIG. 5. The solid lines are the experimental values of $d\epsilon_1/dE$ and $d\epsilon_2/dE$. The dashed lines are fits to Eq. (A16).

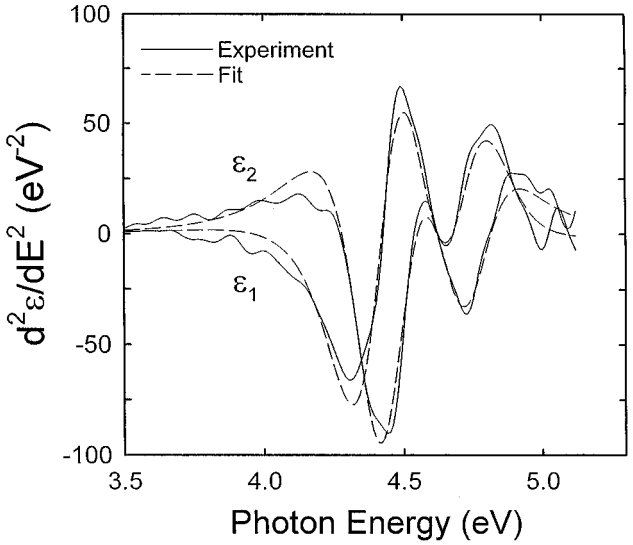

FIG. 6. The solid lines are the experimental values of $d^2\epsilon_1/dE^2$ and $d^2\epsilon_2/dE^2$. The dashed lines are fits to Eq. (A17).

the addition of *ad hoc* terms, such as a Gaussian broadening (in addition to the Lorentzian),[10,31] in order to properly account for the experimental data.

Our value for $R_0 = 20$ meV (Table I) is somewhat larger than that reported for ZnSe. Based on the smaller band gap of $Zn_xCd_{1-x}Se/InP$ in relation to ZnSe one would have expected a somewhat smaller exciton binding energy. The value of $R_1 = 270 \pm 50$ meV is in good agreement with the theoretical calculation of 300 meV in Ref. 28.

The small feature at about 2.1 eV in the data of Fig. 4 is probably due to an exciton longitudinal-optical phonon resonance, as discussed by Trallero-Giner *et al.*[32] It was not explicitly included in our calculation.

The broadening parameter for both the exciton and band-to-band E_0 transition is comparable to that reported by Kim and Sivananthan[10] for ZnSe and quite a bit narrower in relation to the ZnSe data of Ref. 8. This is evidence for the high quality of our alloy sample.

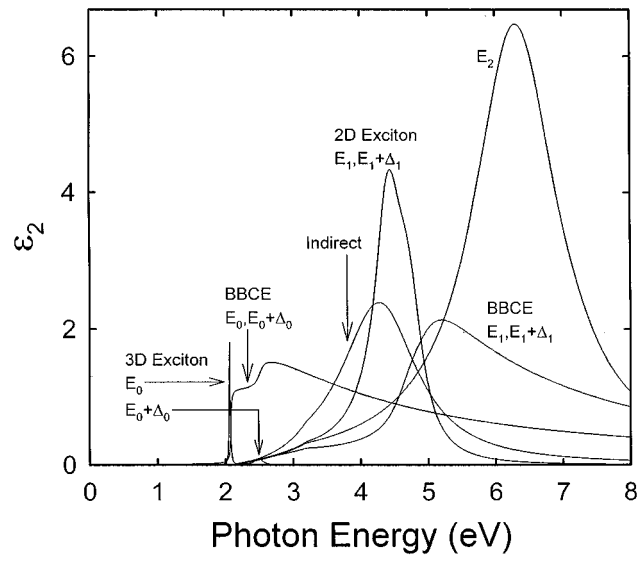

FIG. 7. Individual contributions of the various transitions to ϵ_2.

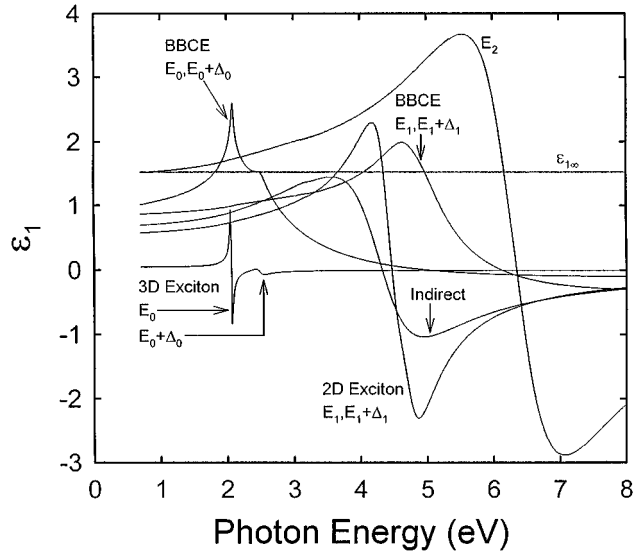

FIG. 8. Individual contributions of the various transitions to ϵ_1.

In order to fit the data between $E_0, E_0+\Delta_0$ and $E_1, E_1+\Delta_1$ we added the contribution of the Γ_8^v-L_6^c indirect transition. Although most authors have not used the Γ_8^v-L_6^c indirect transition to fit their data for direct band-gap materials, such as ZnSe, Adachi did employ it for his analysis of InP.[29] It should be mentioned that in $Zn_xCd_{1-x}Se$/InP the separation between $E_0, E_0+\Delta_0$ and $E_1, E_1+\Delta_1$ is about 300 meV larger than in ZnSe (see Table I). Therefore, any deficiencies in the model dielectric function, such as the assumption of parabolic bands, are more likely to appear in this material. This may also be the reason why it was necessary to add another oscillator in the region between these major spectral structures.

V. SUMMARY

In summary, we have measured the optical constants of $Zn_{0.53}Cd_{0.47}Se$/InP in the range 0.8–5.5 eV. Our data exhibit four distinct CP structures which have been fit using a model dielectric function which includes excitonic and relevant BBCE profiles for not only $E_0, E_0+\Delta_0$ but also for $E_1, E_1+\Delta_1$. Because of sharpness of our spectra, related to the high quality of our samples, we have been able to extract a number of important materials parameters, including excitonic binding energies at both $E_0, E_0+\Delta_0$ and $E_1, E_1+\Delta_1$ as well as the influence of the Γ_8-L_6 indirect transition. The values of the various parameters in Table I are somewhat different from those reported in Ref. 6 because of the extended range of the photon energy of this work in relation to the prior study. The effects of the native oxide on the optical properties has been examined. We find the thickness of this oxide to be ≈ 20 Å.

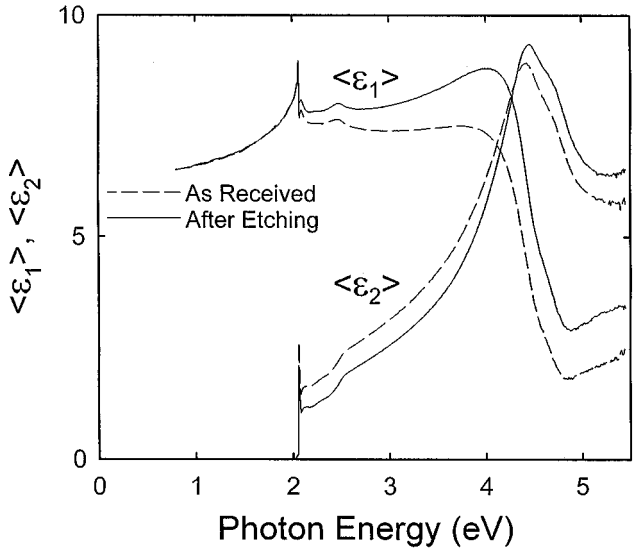

FIG. 9. The solid lines are $\langle \epsilon_1 \rangle$ and $\langle \epsilon_2 \rangle$ for the as-received sample (native oxide). The dashed lines are ϵ_1 and ϵ_2 after removal of the oxide.

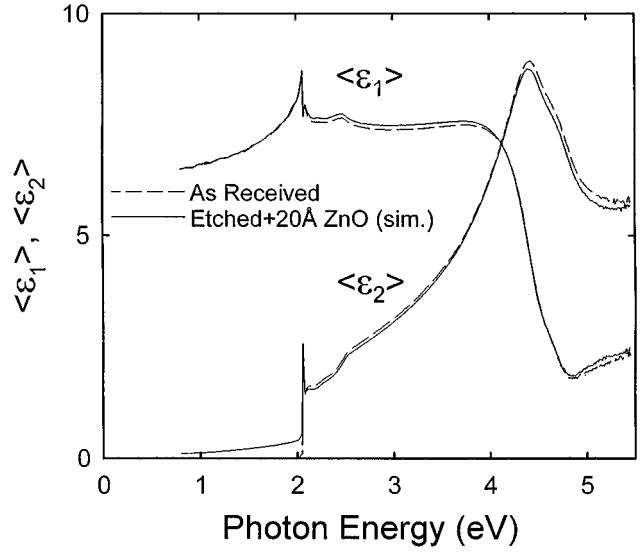

FIG. 10. The solid lines are $\langle \epsilon_1 \rangle$ and $\langle \epsilon_2 \rangle$ for the as-received sample (native oxide). The dashed lines are a simulation of $\langle \epsilon_1 \rangle$ and $\langle \epsilon_2 \rangle$ with 20 Å of ZnO.

ACKNOWLEDGMENTS

T.H. and F.H.P. wish to thank the support of U.S. Army Research Office Contract No. DAAHO4-94-G-0153, National Science Foundation Grant No. DMR-9414209, and PSC/BHE Grant No. 666424. B.X.Y and M.C.T. acknowledge the support of National Science Foundation Grant No. ECS-9320415 and the National Science Foundation Minority Research Center of Excellence under cooperative agreement No. RII-935488. All authors wish to thank the New York State Science and Technology Foundation through its Centers for Advanced Technology program for assistance in this project.

APPENDIX

To evaluate the integral in Eq. (2a) we follow the method presented in Gõni *et al.*[24] First, the exponentials can be rewritten as

$$\frac{1}{1-e^{-2\pi z}} = \frac{1}{2}[1+\coth(\pi z)]. \tag{A1}$$

The terms resulting from the first term on the right side of the above equation can be integrated directly and yield

$$-\tfrac{1}{2}\ \mathrm{Im}\{\ln[(E_0-E-i\Gamma)(E_0+E+i\Gamma)]\}, \tag{A2}$$

while those corresponding to the $\coth(\pi z)$ factor can be transformed via

$$x_1^2=z_1^{-2}=\frac{E'-E_0}{R_0},\quad \xi_1^2=\frac{E_0-E-i\Gamma}{R_0}, \tag{A3}$$

and

$$x_2^2=z_2^{-2}=\frac{E'+E_0}{R_0},\quad \xi_2^2=\frac{E_0+E+i\Gamma}{R_0}, \tag{A4}$$

to give

$$\mathrm{Im}\left[\int_0^\infty dx\ \frac{x}{x_1^2+\xi_1^2}\coth\left(\frac{\pi}{x_1}\right)-\int_0^\infty dx\ \frac{x}{x_2^2+\xi_2^2}\coth\left(\frac{\pi}{x_2}\right)\right], \tag{A5}$$

which is an even function which can be solved by contour integration. The poles in the upper hemisphere are

$$x=i\xi\quad\text{and}\quad x=\frac{i}{m},\quad m=1,2,3,\ldots\ . \tag{A6}$$

Following this integration, the total dielectric function can be determined from the KK relation to be

$$\epsilon(E)=\frac{A}{2E^2}\left\{\sum_{n=1}^{\infty}\{gb_n[\xi(E+i\Gamma_n)]+gb_n[\xi(-E-i\Gamma_n)]-gb_n[\xi(i\Gamma_n)]-gb_n[\xi(-i\Gamma_n)]\}+gu[\xi(E+i\Gamma_0)]\right.$$
$$\left.+gu[\xi(-E-i\Gamma_0)]-gu[\xi(i\Gamma_0)]-gu[\xi(-i\Gamma_0)]\right\}, \tag{A7}$$

where

$$\xi^2(X)=\frac{E_0-X}{R}, \tag{A8}$$

$$gb_n(\xi)=\frac{4}{n^3}\frac{1}{\xi^2-1/n^2}, \tag{A9}$$

$$gu(\xi)=-\ln(\xi^2)-\pi\cot\left(\frac{\pi}{\xi}\right)-\sum_{n=1}^{\infty}\frac{2}{n^3}\frac{1}{\xi^2-1/n^2}, \tag{A10}$$

with gb corresponding to the bound excitonic states and gu to the unbound continuum states (BBCE). The terms involving $\xi(i\Gamma)$ and $\xi(-i\Gamma)$ only contribute to ϵ_1 as they are complex conjugates of each other.

Equation (A7) corresponds closely to expressions given by other authors.[23,24] However, it has the advantage of containing both dielectric functions and being easier to work with analytically as it involves only algebraic and trigonometric functions.

The expression for the E_1 2D critical point can be broadened in much the same way except now one uses the relation

$$\frac{1}{1+e^{-2\pi z}}=\frac{1}{2}[1+\tanh(\pi z)]. \tag{A11}$$

The broadened function can then be written as

$$\epsilon(E)=\frac{C}{2E^2}\left\{\sum_{n=1}^{\infty}\{gb_n[\xi(E+i\Gamma)]+gb_n[\xi(-E-i\Gamma)]-gb_n[\xi(i\Gamma)]-gb_n[\xi(-i\Gamma)]\}+gu[\xi(E+i\Gamma)]\right.$$
$$\left.+gu[\xi(-E-i\Gamma)]-gu[\xi(i\Gamma)]-gu[\xi(-i\Gamma)]\right\}, \tag{A12}$$

where now

$$\xi^2(X)=\frac{4(E_0-X)}{G}, \tag{A13}$$

$$gb_n(\xi)=\frac{32}{(2n-1)^3}\frac{1}{\xi^2-4/(2n-1)^2}, \tag{A14}$$

$$gu(\xi) = -\ln(\xi^2) + \pi \tan\left(\frac{\pi}{\xi}\right) - \sum_{n=1}^{\infty} \frac{16}{(2n-1)^3} \frac{1}{\xi^2 - 1/(2n-1)^2}. \tag{A15}$$

The first and second derivatives of the dielectric function with respect to energy can be written as

$$\frac{d\epsilon}{dE} = \frac{-2\varepsilon}{E} + \frac{4C}{GE^2} \left\{ \left[\frac{1}{\xi_1^2} - \frac{1}{\xi_2^2} \right] + \frac{\pi^2}{2} \left[\frac{1}{\xi_1^3} \sec^2\left(\frac{\pi}{\xi_1}\right) - \frac{1}{\xi_2^3} \sec^2\left(\frac{\pi}{\xi_2}\right) \right] \right.$$
$$\left. + \sum_{m=1}^{\infty} \frac{16}{(2m-1)^3} \left[\frac{1}{\left(\xi_1^2 - \frac{4}{(2m-1)^2}\right)^2} - \frac{1}{\left(\xi_2^2 - \frac{4}{(2m-1)^2}\right)^2} \right] \right\} \tag{A16}$$

and

$$\frac{d^2\epsilon}{dE^2} = \frac{-2\epsilon}{E^2} - \frac{2}{E}\frac{d\varepsilon}{dE} + \frac{16C}{G^2E^2} \left\{ \left[\frac{1}{\xi_1^4} + \frac{1}{\xi_2^4} \right] + \frac{3\pi^2}{4} \left[\frac{1}{\xi_1^5} \sec^2\left(\frac{\pi}{\xi_1}\right) + \frac{1}{\xi_2^5} \sec^2\left(\frac{\pi}{\xi_2}\right) \right] + \frac{\pi^3}{2} \left[\frac{\sec^2\left(\frac{\pi}{\xi_1}\right)\tan\left(\frac{\pi}{\xi_1}\right)}{\xi_1^6} \right.\right.$$
$$\left.\left. + \frac{\sec^2\left(\frac{\pi}{\xi_2}\right)\tan\left(\frac{\pi}{\xi_2}\right)}{\xi_2^6} \right] + \sum_{m=1}^{\infty} \frac{32}{(2m-1)^3} \left[\frac{1}{\left(\xi_1^2 - \frac{4}{(2m-1)^2}\right)^3} + \frac{1}{\left(\xi_2^2 - \frac{4}{(2m-1)^2}\right)^3} \right] \right\}, \tag{A17}$$

with $\xi_1 = \xi(E + i\Gamma)$ and $\xi_2 = \xi(E - i\Gamma)$.

---

*Also at the Graduate School and University Center of the City University of New York, New York, NY 10036.

†Electronic address: FHPBC@CUNYVM.CUNY.EDU

[1] M. A. Haase, J. Qiu, J. M. Depuydt, and H. Cheng, Appl. Phys. Lett. **59**, 1272 (1991); H. Jeon, J. Ding, W. Xie, M. Kobayashi, R. L. Gunshor, and A. V. Nurmikko, *ibid.* **59**, 3619 (1991); G. F. Nuemark, R. M. Park, and J. M. DePuydt, Phys. Today **47 (6)**, 26 (1994).

[2] A. Ishibashi (unpublished).

[3] G. Guha, J. M. DePuydt, J. Liu, G. E. Hofler, M. A. Haase, B. J. Wu, and H. Cheng, Appl. Phys. Lett. **63**, 3023 (1993).

[4] L. H. Kuo, L. Salananca-Riba, B. J. Wu, G. Hofer, J. M. DePuydt, and H. Cheng, Appl. Phys. Lett. **67**, 3298 (1995).

[5] L. Malikova, W. Krystek, F. H. Pollak, N. Dai, A. Cavus, and M. C. Tamargo, Phys. Rev. B **54**, 1819 (1996).

[6] T. Holden, P. Ram, F. H. Pollak, J. L. Freeouf, B. X. Yang and M. C. Tamargo, in *Proceedings of the 23rd International Conference on the Physics of Semiconductors, Berlin, 1996*, edited by M. Scheffler and R. Zimmermann (World Scientific, Singapore, 1996), p. 289.

[7] F. Herman, R. L. Kortum, C. D. Kuglin and J. L. Shay, *Proceedings of the 1967 International Conference on II-VI Semiconducting Compounds*, edited by D. G. Thomas (Benjamin, New York, 1967), p. 503.

[8] S. Adachi and T. Taguchi, Phys. Rev. B **43**, 9569 (1991).

[9] R. Dahmani, L. Salamanca-Riba, N. V. Nguyen, D. Chandler-Horowitz, and B. T. Jonker, J. Appl. Phys. **76**, 514 (1994).

[10] C. C. Kim and S. Sivananthan, Phys. Rev. B **53**, 1475 (1996).

[11] Y. D. Kim, S. L. Cooper, M. V. Klein, and B. T. Jonker, Appl. Phys. Lett. **62**, 2387 (1993).

[12] Y. D. Kim, M. V. Klein, S. F. Ren, Y. C. Chang, H. Luo, N. Samarth, and J. K. Furdyna, Phys. Rev. B **49**, 7262 (1994).

[13] J. Lee, B. Hong, J. S. Burnham, R. W. Collins, F. Flack, and N. Samarth, in *Diagnostic Techniques for Semiconductor Materials Processing II*, edited by S. W. Pang *et al.*, MRS Symposia Proceedings No. 406 (Materials Research Society, Pittsburgh, 1996), p. 377.

[14] J. Lee, B. Hong, R. W. Collins, A. R. Heyd, F. Flack, and N. Samarth, Appl. Phys. Lett. **69**, 2273 (1996).

[15] S. Ninomiya and S. Adachi, J. Appl. Phys. **78**, 4681 (1995).

[16] B. X. Yang, L. Zeng, A. Cavus, M. C. Tamargo, E. Snoeks, and L. Zhao (unpublished).

[17] D. E. Aspnes, in *Optical Properties of Solids: New Developments*, edited by B. O. Seraphin (North-Holland, New York, 1976), p. 799.

[18] O. Acher, E. Bigan, and B. Drévillon, Rev. Sci. Instrum. **60**, 65 (1989).

[19] U. Rossow and W. Richter, in *Optical Characterization of Epitaxial Semiconductor Layers*, edited by G. Bauer and W. Richter (Springer, Berlin, 1996), p. 68.

[20] L. M. Liu *et al.*, J. Vac. Sci. Technol. B **13**, 2238 (1995).

[21] F. A. Jenkins and H. E. White, *Fundamentals of Optics*, 3rd ed. (McGraw-Hill, New York, 1957), p. 472.

[22] J. R. Chelikowsky and M. L. Cohen, Phys. Rev. B **14**, 556 (1976).

[23] R. J. Elliot, Phys. Rev. **108**, 1384 (1957).

[24] A. R. Gõni, A. Cantarero, K. Syassen, and M. Cardona, Phys. Rev. B **41**, 10 111 (1990).

[25] C. Tanguay, Phys. Rev. Lett. **75**, 4090 (1995).

[26] C. Tanguay, Solid State Commun. **98**, 65 (1996).
[27] R. Zimmermann, Jpn. J. Appl. Phys. 1 **34**, 228 (1995).
[28] Y. Petroff and M. Balkanski, Phys. Rev. B **3**, 3299 (1971).
[29] S. Adachi, *Physical Properties of III-V Semiconductor Compounds* (Wiley, New York, 1992).
[30] M. Chandrasekhar and F. H. Pollak, Phys. Rev. B **15**, 2127 (1977).
[31] C. C. Kim, J. W. Garland, and P. M. Raccah, Phys. Rev. B **45**, 11 749 (1992); **47**, 1876 (1993).
[32] C. Trallero-Giner, R. Zimmermann, M. Trinn, and R. Ulbrich, in *Proceedings of the 23rd International Conference on the Physics of Semiconductors, Berlin, 1996* (Ref. 6), p. 345.